Earth-Science Reviews 197 (2019) 102917

Contents lists available at ScienceDirect

Earth-Science Reviews

journal homepage: www.elsevier.com/locate/earscirev

Response and feedback of the Indian summer monsoon and the Southern Westerly Winds to a temperature contrast between the hemispheres during the last glacial–interglacial transitional period

Bing Hong[a,b,*], Jorge Rabassa[c], Masao Uchida[d], Yetang Hong[a,*], Haijun Peng[a], Hanwei Ding[a], Qian Guo[a], Hu Yao[a]

[a] State Key Laboratory of Environmental Geochemistry, Institute of Geochemistry, Chinese Academy of Sciences, 99 Lincheng Road West, Guiyang, Guizhou 550081, China
[b] CAS Center for Excellence in Quaternary Science and Global Change, Xi'an 710061, China
[c] Centro Austral de Investigaciones Cientificas (CADIC, CONICET), C.C. 92, 9410 Ushuaia, Tierra del Fuego, Argentina
[d] Center for Environmental Measurement and Analysis, National Institute for Environmental Studies, Onogawa 16-2, Tsukuba, Ibaraki 305-0053, Japan

ARTICLE INFO

Keywords:
Earth system
Interhemispheric thermal gradient
Meridional overturning circulation
ENSO
ITCZ
Patagonia
Peat

ABSTRACT

The hypothesis that an interhemispheric thermal gradient, or a temperature contrast between the hemispheres (TCBH), drives shifts in the latitudinal position of the Intertropical Convergence Zone (ITCZ) and the Southern Westerly Winds (SWW) is considered one of the most important climate change mechanisms proposed in the last few decades. However, the controversy over the shifting magnitude and direction of the ITCZ and the SWW brings uncertainty to the hypothesis. Here, we further examine the shifting characteristics of the ITCZ and its relationship with the intensity variation of the Indian summer monsoon (ISM) based on synthesis and summary of previously published literature data. In particular, we evaluate regional distribution patterns of the dry and wet climatic changes in southern South America during the last glacial–interglacial transitional period, including the Heinrich event 1, the Antarctic Cold Reversal, and the Younger Dryas. The results show that in response to the Northern Hemisphere-wide cooling and the Southern Hemisphere-wide warming (the Northern Hemisphere-wide warming and the Southern Hemisphere-wide cooling) during the period, the ITCZ over the Asian and northern South American continents and the SWW shift poleward (equatorward), while the intensity of the ISM decreases (increases). However, the shifting characteristics of the ITCZ over the vast Pacific Ocean remain unclear, which implies that the relationship between the TCBH and the El Niño-Southern Oscillation in the tropical Pacific Ocean needs to be studied. In addition, there may be a relatively stable core region in the SWW. This core region is located in Central Patagonia at approximately 47°S, where the local climate is wetter during the all transition period, showing the continuous influence of the SWW on this region. The position shift of the SWW in response to the TCBH phase changes seems to behave as a swing process with an axis of approximately 47°S. The poleward swing of the SWW may trigger the self-repairing process of the global climate system after the catastrophic impacts of the meltwater, including the pulling effect of the enhanced upwelling on the Atlantic meridional overturning circulation, the influence of CO_2 released from the deep sea, and the impact of the gradual strengthening of the ISM. These results support and reinforce the hypothesis that the TCBH drives global climate change, highlight the global teleconnection characteristics of the key physical processes in the Earth's climate system and the important role of the SWW in this teleconnection, and provide a basis for further simulating the climate connections in the two hemispheres, especially the impact of the SWW on the global climate change.

1. Introduction

The Indian summer monsoon (ISM), originating from the middle latitudes of the Southern Hemisphere (SH), transports water vapour to the Northern Hemisphere (NH) when it crosses the equator, which exerts a great influence on the food and livelihood of almost one-half of

* Corresponding authors at: State Key Laboratory of Environmental Geochemistry, Institute of Geochemistry, Chinese Academy of Sciences, 99 Lincheng Road West, Guiyang, Guizhou 550081, China.
E-mail addresses: hongbing@vip.skleg.cn (B. Hong), hongyetang@vip.skleg.cn (Y. Hong).

https://doi.org/10.1016/j.earscirev.2019.102917
Received 3 April 2019; Received in revised form 25 July 2019; Accepted 26 July 2019
Available online 26 July 2019
0012-8252/

the world's population through monsoon rainfall. The Southern Westerly Winds (SWW) drive upwelling near Antarctica, which has been considered an important force that releases CO_2 from the deep ocean interior into the atmosphere (Toggweiler et al., 2006; Anderson et al., 2009; Denton et al., 2010). Advances in research on the response of the ISM to millennial-scale climate variations in high northern latitudes during the last deglaciation (Yuan et al., 2004) and the Holocene (Fleitmann et al., 2003; Gupta et al., 2003; Hong et al., 2003; Wang et al., 2005; Dykoski et al., 2005) have provided valuable information on monsoon mechanisms. However, correlations between the ISM and high southern latitude climates, particularly between the ISM and the SWW, during the last deglaciation and the Holocene are not well understood. Along with the deepening of global climate teleconnection research, the relationship between the ISM and SWW has attracted more and more attention. Over the past 20 years, observations and models have led to the emergence of the hypothesis that millennial-scale shifts in the Atlantic meridional overturning circulation (AMOC) have redistributed heat among the earth's systems and promoted systematic changes in the global climate during the most recent glacial and interglacial periods. An abrupt reduction in the strength of the AMOC in the high-latitude North Atlantic promoted an immediate decrease in the northward heat transport. This change resulted in the surface air temperature decreasing over the North Atlantic and increasing over the South Atlantic, which led to the formation of an interhemispheric thermal gradient, or a temperature contrast between the hemispheres (TCBH). These changes were also accompanied by a southward or poleward shift of both the intertropical convergence zone (ITCZ) and the SWW, the decline of the ISM, and an intensification of the Antarctic circumpolar current (Broecker et al., 1985; Broecker, 1994; Alley et al., 1999; Knutti et al., 2004; Barker et al., 2009; Chiang and Friedman, 2012; Landais et al., 2015). Thus, the TCBH refers to the surface temperature contrast between the two hemispheres characterized by the $\delta^{18}O$ values of the ice cores at the two poles of the Earth, although the TCBH appears to be relatively flat (Toggweiler, 2009). In this study, we use the term 'positive TCBH' to denote this type of TCBH, that is, the NH-wide cooling and the SH-wide warming. Conversely, the term "negative TCBH" is used to denote the NH-wide warming and the SH-wide cooling. According to this hypothesis, there seems to be some kind of connection between the ITCZ, ISM, and SWW, but this possible connection remains obscure as the details of the ITCZ and SWW shifts are still controversial. Stager et al. (2011) questioned that to explain the broad geographic range of the severe drought in Africa and Asia during the period from approximately 16,000 to 17,000 cal yr BP, the latitudinal displacement of the ITCZ must generally be unrealistically large, on the order of 20 degrees of latitude or more (Stager et al., 2011). McGee et al. (2014) also suggest that past shifts in the zonal-mean ITCZ position are likely to be small. The mean shifts in the ITCZ are approximately less than 1 degrees of latitude during the Last Glacial Maximum (LGM), Heinrich Stadial 1, and mid-Holocene. McGee et al. (2014) further suggest that "Large ($\geqq 5^{\circ}$) meridional displacements of the ITCZ inferred from regional compilations of proxy records must be limited in their zonal extent, and ITCZ shifts at other longitudes must be near zero, for the global mean shift to remain $\leqq 1^{\circ}$ as suggested by our results." A recent study shows that the globally zonal-mean position of ITCZ has remained approximately constant over the past decades, although observations and reanalysis data show a narrowing and strengthening of precipitation in the ITCZ (Byrne et al., 2018). In addition, the understanding of the direction and magnitude of the shift of the SWW in geological history is also controversial (Moreno et al., 2012; Kohfeld et al., 2013). Therefore, further clarifying the relationship among the ITCZ, ISM and SWW in response to changes in the TCBH has become an important step in testing and strengthening the above hypothesis.

For this purpose, we further examine the shifting characteristics of the latitudinal position of the ITCZ and the relationship between the latitudinal position of ITCZ and the ISM intensity variation during the last deglaciation period based on the synthesis and summary of previously published data. Considering the important effects of the El Niño-Southern Oscillation (ENSO) activity in the tropical Pacific Ocean on the ITCZ and ISM, we also discuss the possible relationship between the ENSO activity and TCBH. In particular, we reveal the evolution pattern of the core position shift of the SWW in response to the changes in the TCBH during the last glacial–interglacial transitional period (approximately 17,000–11,000 cal yrs. BP). Through a comprehensive comparison of the above aspects, the teleconnections between the ITCZ, ISM, SWW, and TCBH were revealed, and the self-repairing process of the Earth's climate system triggered by the SWW is proposed. These results will contribute to a better understanding of the correlation and interaction mechanisms of key physical processes in the Earth's climate system.

2. Material and methods

The ITCZ is a large-scale's atmospheric circulation system in the low latitude atmosphere on the Earth, and is defined as a convergence zone in the low pressure trough (the equatorial trough) between the southeast and the northeast trade winds. The ITCZ shows as a narrow and approximately continuous convective cloud band near the Earth's equator on satellite images, therefore, is also the band area with the maximum in time-mean precipitation on the Earth (Fig. 1). The zonal-mean position of the ITCZ is consistent with the rising branch of the global Hadley cell.

Over the Indian Ocean and adjacent land surfaces, precipitation occurs almost entirely within an ITCZ (Mohtadi et al., 2016). Therefore, a seasonal migration of the ITCZ resulted from the cross-equatorial pressure gradients prompts the seasonal rainfall variations of the ISM, which also serves as the basis for trying to understand the history of the ITCZ migration based on the variation of the ISM in geological history. The SWW associated with the Southern Annular Mode (Fletcher and Moreno, 2011) is an integral part of the atmospheric circulation system in the SH. Because the SWW is banded and distributed over the mid-latitudes of the SH, it is also known as the SWW belt. When the SWW runs westward across the South American continent between approximately 37° and 56°S, which is the region known as Patagonia, the SWW transports water vapour from the South Pacific to the windward side of the Andean Cordillera, forming abundant precipitation. On the eastern side of the Andes, the amount of precipitation decreases rapidly with distance from the Pacific coast (Garreaud, 2007; Moreno et al., 2012), which shows that the precipitation in the mountainous areas of the Andean Cordillera, including its eastern and western slopes, is affected mainly by the SWW. Precipitation in the extra-Andes region and the Atlantic seaboard may be affected by the water vapour from the Atlantic and the influence of water vapour from the South Pacific (Moreno et al., 2012), although the exact relative contribution of the two kinds of water vapour sources and the corresponding spatial changes are not clear.

To further understand the response of the ITCZ, ISM and SWW to the TCBH during the last glacial-interglacial transition, we synthesized and evaluated the previously published paleoclimatic records on the basis of field investigations. We considered that the relevant paleoclimatic records used for this study should meet the following conditions: they were published in peer-reviewed professional journals and they had a credible dating technique and presented the calibrated (calendar) age. These paleoclimate records should provide the climate information associated with the ISM and SWW during the periods of the Heinrich event 1 (H1, ~16.7–15.0 cal kyr BP), the Antarctic Cold Reversal (ACR, ~14.5–13.0 cal kyr BP), and the Younger Dryas (YD, ~12.8–11.6 cal kyr BP) events or during the periods roughly equivalent to the main time intervals of the events mentioned above. In order to accurately understand the evolution history of the SWW, only the research sites on the western side of the Andes and on the eastern slope of the mountains were used in this study, because the water vapour of rainfall in these

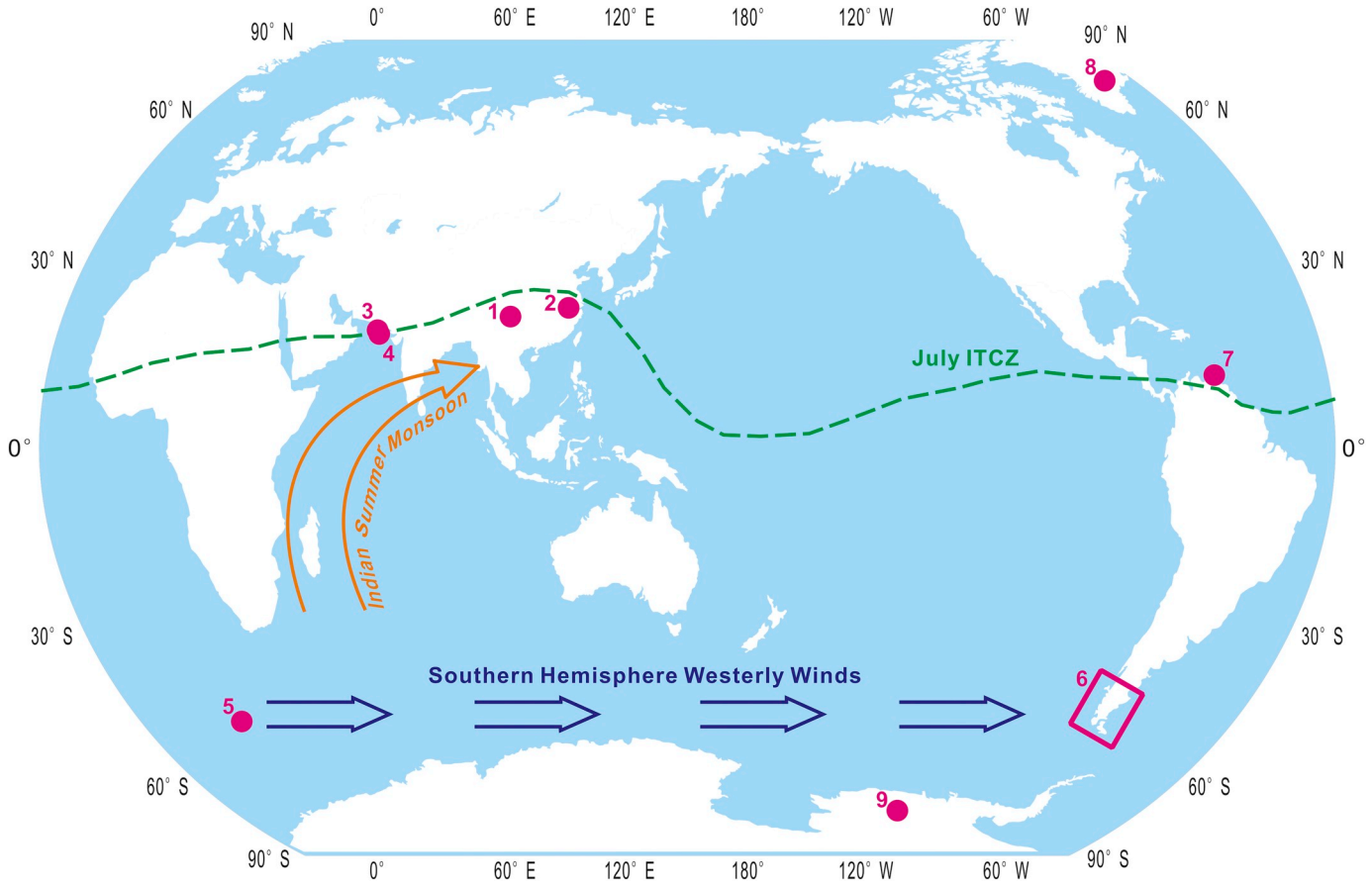

Fig. 1. Map showing the relative research sites for this study and sketches of the Indian summer monsoon, the Southern Hemisphere westerly winds, and the Intertropical Convergence Zone. 1–Yuexi peat bog (Hong et al., 2018). 2–Hulu cave (Wang et al., 2001). 3–Northeastern Arabian Sea core (Deplazes et al., 2013). 4–136 KL core (Schulz et al., 1998). 5–TN057-13-4PC core (Anderson et al., 2009). 6–The study area in the southern South America (this study, Table 1). 7–The Cariaco Basin (Deplazes et al., 2013). 8–The Greenland Ice Sheet Project Two (GISP2) ice core (Stuiver and Grootes, 2000). 9–Byrd ice core in Antarctica (Blunier and Brook, 2001). Dashed lines show the modern position of the Intertropical Convergence Zone in July (modified from reference Cheng et al., 2012).

Table 1
Palaeoclimatic records from 14 sites in the southern South America (abbreviations see below).

Number	Research site	Location	Archive	Proxy indicator	Dating		Reference
					Meth.	No.	
1	GeoB 3302–1 core (Water depth 1498 m)	33°13′S ; 72°06′W	Marine sediment	M	^{14}C (AMS)	7	Lamy et al., 1999
2	Lago Pichilafquén (218 m a.s.l.)	40°44′S ; 72°28′W	Lake sediment	P, OM, CC, C	^{14}C (AMS)	13	Jara and Moreno, 2014
3	Lago Pichilaguna (110 m a.s.l.)	41°15′S ; 73°03′W	Lake sediment	P, C, CM, OM, MS	^{14}C (AMS)	29	Moreno et al., 2018
4	Lago Lepué, (124 m a.s.l.)	42°48′S ; 73°42′W	Lake sediment	P, OM, CC, C	^{14}C (AMS)	27	Pesce and Moreno, 2014
5	Lago Los Niños (1015 m a.s.l.)	44°0.1′S ; 71°17′W	Lake sediment	P, MS, CC, C	^{14}C (AMS)	16	Iglesias et al., 2016
6	Mallín Pollux, (640 m a.s.l.)	45°41′ S, 71°50′ W	Fen sediment	P, C, MS	^{14}C (AMS)	20	Markgraf et al., 2007
7	Lago Augusta (440 m a.s.l.),	47°05′S ; 72°23′W	Lake sediment	P, C, OM, CC	^{14}C (AMS)	8	Villa-Martínez et al., 2012
8	Lago Edita (570 m a.s.l.),	47°08′S ; 72°25′W	Lake sediment	P, C, OM, CC	^{14}C (AMS)	5	Henríquez et al., 2017
9	Pantano Dumestre (77 m a.s.l.),	51°48′S ; 72°26′W	Bog sediment	P, C, OM, CC, SD	^{14}C (AMS)	8	Moreno et al., 2012
10	Laguna Potrok Aike (113 m a.s.l.),	51°58′S ; 70°23′W	Lake sediment	P, C, D, GA	^{14}C (AMS)	16	Wille et al., 2007
11	Rio Rubens	52°04′S ; 71°31′W	Bog sediment	P, C	^{14}C	19	Markgraf and Uber, 2010
12	Punta Yartou core (51 m a.s.l.)	53°51′S; 70°08′W	Mire sediment	P, C	^{14}C (AMS)	15	Mansilla et al., 2016
13	La Correntina mire (206 m a.s.l.)	54°33′S; 66°59′W	Mire sediment	P	^{14}C (AMS)	7	Musotto et al., 2017
14	Harberton (20 m a.s.l.)	54°54′S, 67°10′W	Peat	P, C	^{14}C	29	Markgraf and Uber, 2010

Proxy indicator: C–charcoal; CC–carbonate content; CM–chemical elements; D–diatoms; GA–green algae; M–minerals; MS–magnetic susceptibility; OD–organic density; OM–organic matter content; P–Pollen.

areas mainly came from the SWW. According to the above requirements, several paleoclimatic records were selected. The relevant research sites involved in this study were shown in Fig. 1, which include 14 research sites in southern South America (Table 1). Most of the 14 records used the pollen assemblages from lake or bog sediments as a proxy indicator for the regional rainfall/effective humidity, except for two records that used the mineral composition of the sediments. This requirement allowed us to obtain the necessary compiled data and helped with the comparison. The information obtained on the dry or wet conditions based on the conclusions noted by the original authors of the paleoclimate records or based on the results indicated by the records themselves was marked on a topographic map based on the geographical coordinates of each research site, so that the regional distribution patterns of the climatic dry and wet conditions may be

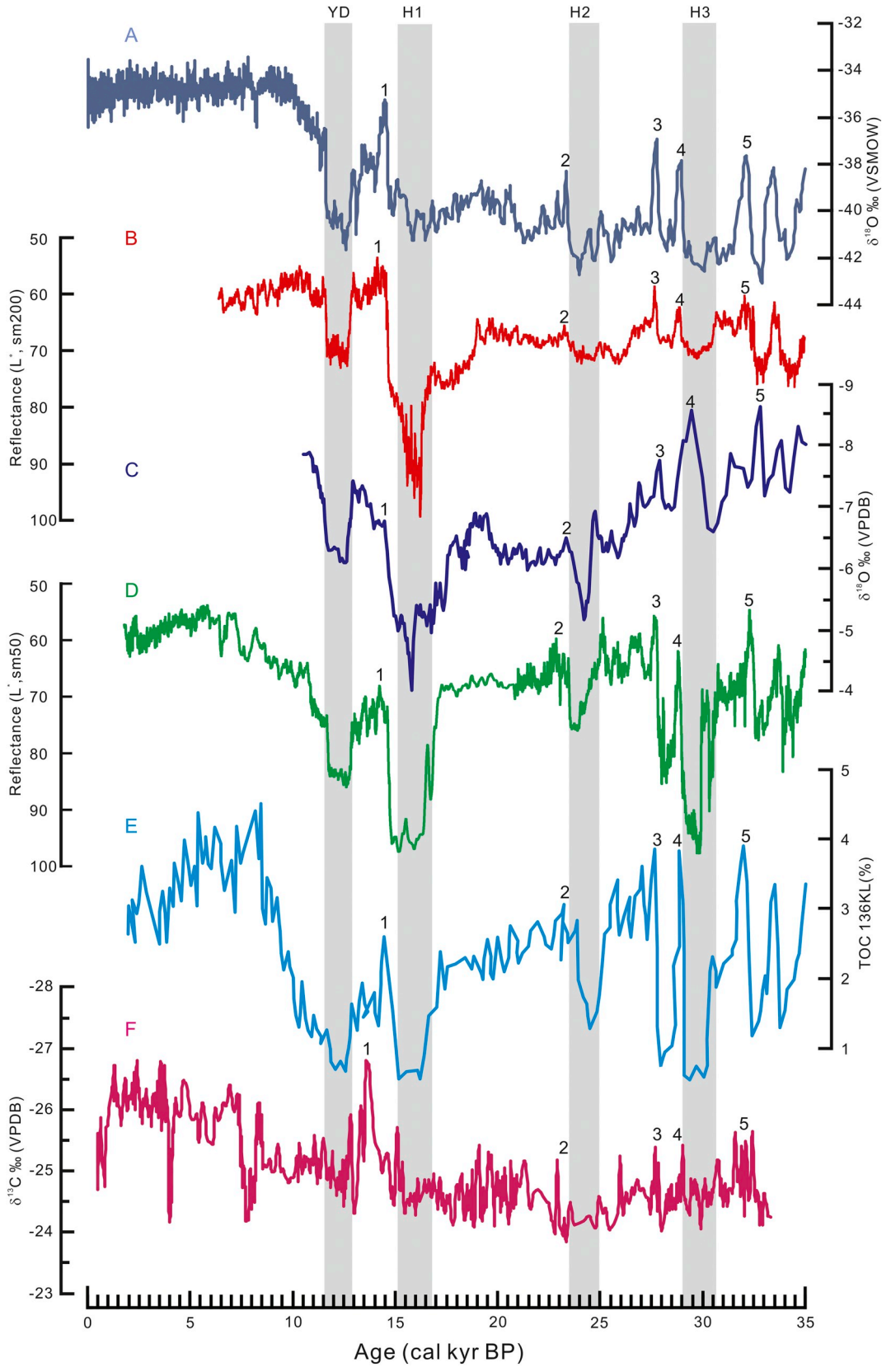

(caption on next page)

Fig. 2. The responses of the Intertropical Convergence Zone, the Indian summer monsoon, and the Southern Hemisphere westerly winds to the high northern latitude climate. A–Temperature record reconstructed from the $\delta^{18}O$ of the GISP2 ice core in Greenland (Stuiver and Grootes, 2000). B–Rainfall record reconstructed from sediment total reflectance (L*) from the Cariaco Basin (Deplazes et al., 2013). C–Rainfall record reconstructed from the $\delta^{18}O$ of stalagmites in Hulu Cave (Wang et al., 2001). D–Rainfall record reconstructed from sediment total reflectance (L*) in the northern Arabian Sea (Site 3 in Fig. 1) (Deplazes et al., 2013). E–Rainfall record reconstructed from the content of total organic carbon in sediment core 136 KL in the northern Arabian Sea (Site 4 in Fig. 1) (Schulz et al., 1998). F–Rainfall record reconstructed from the $\delta^{13}C$ of peat cellulose from Yuexi (Hong et al., 2018). The climatic intervals are abbreviated as follows: YD–Younger Dryas; H1–3–Heinrich events 1–3. Numbers indicate Greenland Interstadials and correlated events at the Cariaco Basin, Hulu, northern Arabian Sea, and Yuexi. The grey bars indicate the YD and Heinrich events.

clearly displayed visually for the time intervals of the H1, the ACR, and the YD events.

3. Results and discussion

3.1. The response of the ITCZ and ISM to the TCBH

Based on the global meteorological data and satellite observations, scientists can now more accurately understand the seasonal and interannual variations of the modern ITCZ. However, the understanding of the shifts of ITCZ in some specific periods of the geological history is still in the process of continuous improvement, because there is usually a lack of a dense network of continuous paleoclimate records with high-resolution (Fleitmann et al., 2007). Since the ITCZ crosses over the Cariaco Basin (Site 7 in Fig. 1) in northern South America, the precipitation record of Cariaco Basin has been used to reflect the historical evolution of the ITCZ position over the region (Deplazes et al., 2013). Figs. 2A and B show the responses of the ITCZ to the TCBH over the Cariaco Basin during the geological history. Corresponding to the cooling events in the high northern latitude region inferred from the light (^{18}O-depleted) $\delta^{18}O$ values in the Greenland GISP2 ice core, including the Heinrich events 3–1 (H3 − H1) and the YD event (Fig. 2A), or to the positive TCBH, the local precipitation inferred from sediment total reflectance (L*) of the Cariaco Basin decreases without exception (Fig. 2B), which is interpreted as reflecting the southward movement of the ITCZ over the Cariaco Basin. In contrast, corresponding to the warming events, including the Bølling-Allerød (B/A) event and the Dansgaard-Oeschger (D/O) oscillations 2–5, or to the negative TCBH, the local rainfall increased, reflecting the northward movement of the ITCZ over the Cariaco Basin. At the same time, Deplazes et al. (2013) also measured the total reflectance (L*) of sediments in the Arabian Sea (Site 3 in Fig. 1) and confirmed Schulz et al.'s previous discovery (Site 4 in Fig. 1) that the intensity of the ISM weakens in response to the cooling events in the high northern latitude region (Figs. 2A,D,E). These findings suggest that the shift of ITCZ over the Arabian Sea is synchronized with that over the Cariaco Basin (Deplazes et al., 2013).

However, whether the shift of ITCZ's position over the Arabian Sea and the Cariaco Basin represents a consistent regional shift pattern of the ITCZ in whole Asia and even in the global still needs to be further proven, because that there is little available research data in the Asian continent and the Pacific region, and in particular, the direction and magnitude of the shifts of the ITCZ over different regions in the Earth may be considerably different, as mentioned in the previous section of this study (McGee et al., 2014). This uncertainty further highlights the need for denser paleoclimate record networks (Fleitmann et al., 2007) so that the response relationship between the shifts of the past ITCZ and the TCBH can be understood more accurately and comprehensively. In the South Asian and the southern continent of East Asia, which is affected by the ISM, the ITCZ crosses over a region with an average latitude of 20°N in the boreal summer (Schneider et al., 2014) (Fig. 1). Thus, this region is a favourable area that can be studied to understand the relationship between the ITCZ over the Asian continent, the ISM rainfall, and the TCBH. The Yuexi peatland developed in this area. This is a valley peat bog at an altitude of 1950 m above sea level, and is located in the Hengduan Mountains at the southeastern edge of the Tibetan Plateau (Site 1 in Fig. 1). The compression of the Indian Plate into the Eurasian Plate resulted in the formation of the Hengduan Mountains, which run in a southwest-northeast direction, and caused the Hengduan Mountains to become a delivery channel for water vapour from the ISM. An investigation of the moisture sources of the June–August precipitation in the Yuexi District and its adjacent region shows that more than 90% of the moisture for summer precipitation originated from the ISM, which supports the previous conclusion that approximately 90% of the moisture flux into southern Asia and its adjacent areas is caused by the cross–equatorial ISM (Hong et al., 2018). The average annual temperature in the Yuexi District is approximately 13 °C, and the mean annual rainfall is approximately 1000 mm. The humid and cool climate of this mountain region has promoted the development of a thick peat sediment layer. Therefore, the peatland in the Hengduan Mountains in southwestern China is ideally positioned to capture ISM signals (Hong et al., 2014, 2018) (Site 1 in Fig. 1). The peat cellulose isotopic ($\delta^{13}C$) record from the Yuexi peatland sensitively reflects the changes in the ISM rainfall (Hong et al., 2001, 2018; Amesbury et al., 2015). Fig. 2 shows that corresponding to the cooling events in the high northern latitude region, including the YD and the H1 − H3 (Fig. 2A), the Yuexi peat record shows an abrupt decrease in the ISM precipitation (Fig. 2F). These results are consistent with the response of the ISM intensity recorded in the sediment of the northern Arabian Sea to the climate changes in the high northern latitude region (Schulz et al., 1998 ; Deplazes et al., 2013), which are interpreted as reflecting a southward shift of the ITCZ in response to the positive TCBH (Figs. 2A, D, E, F). Therefore, the shift direction of the ITCZ over the South Asian and the southern continent of East Asia is consistent with the shift direction of the ITCZ over the northern South American continent, i.e., they all shift southward or poleward during this period. In contrast, corresponding to the warming events, including the B/A event and the D/O oscillations 2–5, or to the negative TCBH, the records from both the Yuexi peat and the Arabian Sea sediment show an abrupt increase in the ISM, indicating the northward shift of the ITCZ over the South Asian and the southern continent of East Asia, which is the same as the migration direction of the ITCZ over the Cariaco Basin. The Hulu Cave record is generally considered to be commonly affected by the ISM and the East Asian summer monsoon (Gao et al., 1962; Pausata et al., 2011; Wang and Chen, 2012; Hong et al., 2014), and also shows similar millennial-scale changes in precipitation. These results show that the zonal-mean position shifts of the ITCZ over the continents on the two sides of the Pacific Ocean are synchronous; furthermore, the directions of their shifts are the same. In response to the positive (negative) TCBH, southward (northward) shifts of the ITCZ over these continents occur.

Due to the lack of available precipitation proxy records, however, the shift of ITCZ over the vast Pacific Ocean was little known during the last deglaciation. The hydrological variations in the tropical West Pacific during the last deglaciation show large regional variability, which leads to various interpretations of the driving mechanism of the regional climate changes (Muller et al., 2008; Griffiths et al., 2009; Shiau et al., 2011; Ayliffe et al., 2013; Denniston et al., 2013; Carolin et al., 2013; Fraser et al., 2014). A recent study suggests that precipitation variations in the tropical West Pacific between 6° and 22° N cannot be explained by a simple meridional shift of the ITCZ during the last glaciation, but, rather, they were related to changes in the regional climate system, including the El Niño-Southern Oscillation (ENSO)

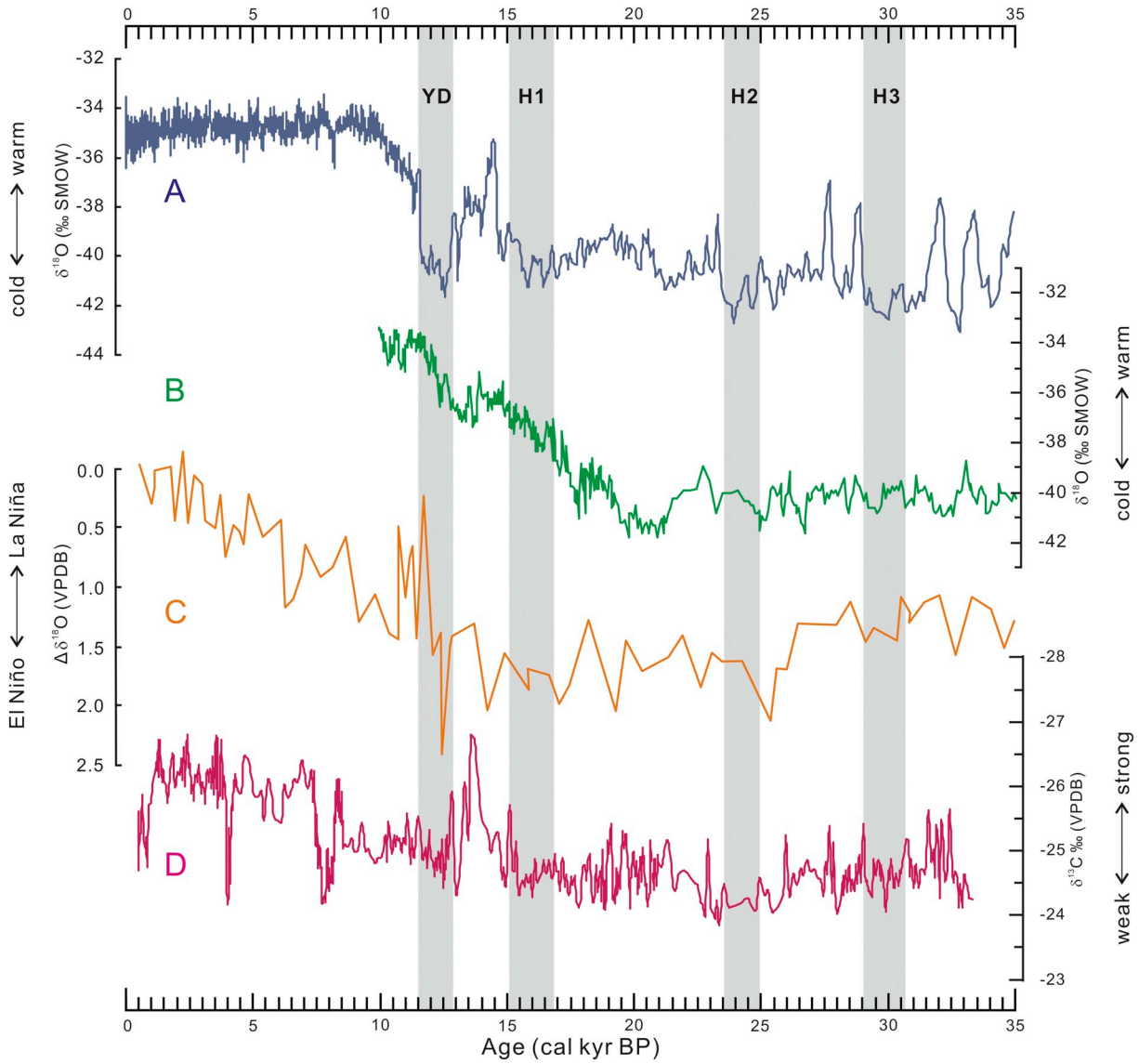

Fig. 3. The relationship among a temperature contrast between the hemispheres (TCBH), the El Niño-Southern Oscillation (ENSO) and the Indian summer monsoon (ISM) during the last deglaciation. A–Temperature record reconstructed from the $\delta^{18}O$ of the GISP2 ice core in Greenland (Stuiver and Grootes, 2000). B–Temperature record reconstructed from the $\delta^{18}O$ of the Byrd ice core in Antarctica (Blunier and Brook, 2001). The comparison of temperature records A and B reflects the condition of TCBH. C–The ENSO activity reconstructed from the salinity variability inferred from the $\Delta\delta^{18}O$ of the planktonic foraminifera (*Globigerinoides ruber*) in the western tropical Pacific warm pool (Stott et al., 2002). D–The ISM record reconstructed from the $\delta^{13}C$ of peat cellulose, Yuexi (Hong et al., 2018). The climatic intervals are abbreviated as follows: YD–Younger Dryas; H1–Heinrich event 1; H2–Heinrich event 2; H3–Heinrich event 3. The grey band indicates the linkages between the positive TCBH, the El Niño-like pattern, and the weakened ISM.

activities related to the AMOC (Xiong et al., 2018). Now we know that the modern ENSO is an abrupt inter-annual shift in the tropical Pacific ocean-atmosphere system that has a significant impact on the abrupt variability of the ISM. Observational and model-based studies have generally suggested that an El Niño (La Niña) warm (cool) configuration over the tropical Pacific Ocean could lead to drought (wet) conditions over the ISM region, thus indicating a weakening (strengthening) of the ISM (Shukla and Paolina, 1983; Webster et al., 1998; Kumar et al., 2006; Meehl and Hu, 2006; Buckley et al., 2010). In addition, the long-term behaviour of the ENSO has been studied over the past decade. Studies of the cold tongue of the eastern equatorial Pacific Ocean have shown that during the YD and the LGM, the sea surface temperature (SST) gradient in the equatorial Pacific Ocean abruptly decreased and the equatorial Pacific Ocean presented a similar pattern to that caused by the modern El Niño (Koutavas et al., 2002). Investigations of the SST and salinity variability in the western tropical Pacific warm pool also led to these results. Millennial-scale El Niño conditions are correlated with stadials at high northern latitudes, and La Niña conditions are correlated with interstadials over the past 70 kyr (Stott et al., 2002) (Fig. 3). These results suggest that the abrupt millennial-scale shifts in the tropical Pacific ocean-atmosphere system during deglaciation may have been analogous to the modern ENSO, and they have been referred to as an ENSO-like pattern (Koutavas et al., 2002; Stott et al., 2002).

We further compared the ENSO-like pattern with the TCBH and explored their impact on the ISM and ITCZ. Fig. 3 shows that the ENSO-like pattern is correlated with the climate in the high northern latitudes, as well as in the high southern latitudes (Figs. 3A, B). The thermal conditions in the equatorial Pacific Ocean may be correlated with the TCBH on a millennial timescale (Stott et al., 2002). During the YD, H1 − H3, the El Niño-like pattern in the equatorial Pacific Ocean corresponded to a positive TCBH, and during the B/A event and D/O warming events, a La Niña-like pattern in the equatorial Pacific Ocean corresponded to a negative TCBH (Figs. 2A, B). Because the TCBH

originated in the AMOC, these correlations may also highlight the AMOC's modulation of the thermal conditions of the equatorial Pacific Ocean. This hypothesis is supported by a simulation that shows a strengthening of ENSO variability when the AMOC is shut down (Timmermann et al., 2007). By combining these results with the results of previous studies (Koutavas et al., 2002; Stott et al., 2002), we suggest that the ENSO-like pattern and the TCBH most likely coupled to form a physical pair of processes associated with the AMOC in the Earth's climate system. Fig. 3 also shows that during a given millennial event, the effect of these two coupled processes on the ISM is not only synchronous on a millennial timescale but also parallel in the driving direction. For instance, the El Niño-like pattern and the positive TCBH simultaneously appeared during the YD, H1 − H3 cold events and played the same role in suppressing the ISM. Similarly, the La Niña-like pattern and the negative TCBH appeared simultaneously during the B/A event, D/O warming events 3–4, and warming event 5 and played the same role in activating the ISM. These results indicate that the TCBH and ENSO seem to have a consistent impact on the ISM and ITCZ in the ISM region, including the Arabian Sea and the Bay of Bengal. But their impact on the ITCZ over the Pacific Ocean is not yet clear. The intensity change of the East Asian summer monsoon related to water vapour from the Pacific Ocean has been reported to be contrary to the intensity change of the ISM (Hong et al., 2005, 2009, 2010, 2014; Maher and Hu, 2006). This inverse correlation was thought to be related to the El Niño-like phenomenon in the tropical Pacific Ocean, resulting in the weakening of the ISM intensity and the strengthening of the East Asian monsoon (Hong et al., 2005, 2009, 2010, 2014). Whether this inverse phase correlation between the two monsoons implies the opposite shift of the ITCZ over the Pacific and Indian Oceans deserved further confirmation, because this opposite change may balance the ITCZ shift over the two oceans and lead to a reduction in the ITCZ global mean shift, as suggested by McGee et al. in 2014. Further elucidation of the ITCZ position shift over the vast Pacific Ocean may be of great significance for revealing the global average position change of the ITCZ and the possible relationship between the ENSO and TCBH during the last deglaciation.

3.2. The response of the position shift of the SWW to the TCBH

Atmospheric precipitation usually shows larger regional variability because there are many factors that affect the precipitation process. Specifically, the influence of terrain factors caused by the Andes Mountains should also be considered in Patagonia (Garreaud, 2007; Moreno et al., 2012). As previous studies have shown, the distribution of the amount of precipitation in western Chile caused by the modern SWW along latitude has quasi-normal distribution characteristics (Lawford, 1996; Quade and Kaplan, 2017). In terms of the mean annual average, the modern maximum precipitation is distributed in the area of approximately 43°–53°S (Moreno et al., 2012; Quade and Kaplan, 2017) (panel A in Fig. 4), which is usually referred to as the core area or the main belt of the SWW and represents the position of the strongest westerly wind. Once the SWW deviates from the core, the amount of precipitation and the intensity of the SWW will rapidly decrease (panel A in Fig. 4). These geographical characteristics of the modern SWW precipitation provide a basis for the reconstruction and interpretation of the historical evolution of the SWW. Based on this, we speculate that in the history of geology, in the areas of Patagonia influenced by the strongest SWW, or in the core area of the SWW, a regional increase in precipitation or a wetter climate pattern should be shown in general, although the occurrence of abnormalities in a few local places would still be expected. The variations in the climatic dry and wet distribution pattern should reflect the shifts of the core position of the SWW during different periods. From the data of 14 research sites distributed in Patagonia and its adjacent areas (Table 1), we try to extract the regional distribution trends of the climatic dry and wet changes during the last glacial–interglacial transition (Fig. 4), which may show the details of the position shifts of the SWW.

A previous study suggested that during the late LGM, the northern edge of the SWW was located in the region north of 40°S (Moreno et al., 1999). At that time, northwest Patagonia was in a cold and hyperhumid climate, reflecting the maximum influence of the SWW (Moreno et al., 2018). Along with the starting of the Last Glacial Termination at 17,800 cal yr BP (Moreno et al., 2018) and the subsequent emergence of H1 event in the NH, the climate in northern Patagonia changed drastically. A marine sediment core (GeoB 3302–1 core, Site 1 in panel H1 in Fig. 4) from the continental slope off mid-latitude Chile (33°S) shows an obvious peak value of coarsening grain size during the period from approximately 17,500 to 15,000 cal yr BP, which is interpreted as a tendency towards a more arid climate condition in the source area of the sediments and a southward shift of the SWW (Lamy et al., 1999). Investigations for several lakes south of the GeoB core in northern Patagonia have also reported climate drying during approximately the same period. For example, palynological study on sediment from Lago Pichilafquén (Site 3 in Fig. 4) shows an abrupt change from hyperhumid to drying climate during the period (Moreno et al., 2018) (Fig. 10 in Moreno et al., 2018). The diagnostic indicator of hydroclimate variations (ECPI) in Lago Lepué region (Site 4 in Fig. 4) shows slightly negative or zero anomalies between 16,100 and 14,600 cal yr BP (Pesce and Moreno, 2014) (Fig. 9 in Pesce and Moreno, 2014), indicating a drier climate in the region. The landscape of the Lago Los Niños region (Site 5 in Fig. 4) is also drier and dominated by heath and steppe taxa characteristic of open ground during approximately the same period, similar to the present-day heath-steppe found today in the wind-blown areas of southern Patagonia (Iglesias et al., 2016). Lago Pollux (Site 6 in Fig. 4) southwest of Lago Los Niños was once a shallow productive pond surrounded by a sparse scrub–steppe during the period from approximately 18,000 to 14,000 cal yr BP, indicating that the local climate in this period was markedly drier (Markgraf et al., 2007). Since the time intervals discussed in the abovementioned studies cover or are roughly equivalent to the interval of the H1 event (from approximately 16,700 to 15,000 cal yr BP), these studies have proved that the climate in northern Patagonia was drier during the H1 event, and the influence of the SWW on precipitation in the area was significantly weakened compared with the influence of the SWW on precipitation in the area in the LGM period. These results are usually interpreted as the southward shift of the mean latitudinal position of the SWW, although the details of the shift, including the magnitude of change and the location of the stop, remain unclear. However, the panel H1 in Fig. 4 shows that the northern edge of the SWW may move to approximately 47°S during the period, because the wetter climate was not recorded until Lago Augusta (Site 7 in Fig. 4) at approximately 47°S in central Patagonia, where hygrophilous rainforest taxa quickly expanded to the Valle Chacabuco Valley in the region (Villa-Martínez et al., 2012). The palynological records from Lago Edita (Site 8 in Fig. 4), which is near Lago Augusta, also suggested that the climate in this region was wetter during the same period (Henríquez et al., 2017). In addition, according to the high water level recorded by Laguna Potrok Aike (Wille et al., 2007) (Site 10 in Fig. 4), and the drier climate in the southernmost part of Patagonia south of Laguna Potrok Aike (Markgraf and Uber, 2010; Mansilla et al., 2016; Musotto et al., 2017) (Sites 11–14 in Fig. 4), the southern margin of SWW may extend southward to approximately 51°S, which may represent the limit of the SWW expansion during the H1 period. The core position of the SWW at that period was almost the same as the core position of the modern SWW (panels H1 and A in Fig. 4). These results provide new evidence for the poleward shift of the SWW that corresponds to the positive TCBH during the H1 event.

After the impact of the H1 event ended, the temperature in Antarctica became cold (an event known as the ACR), the TCBH turned to the negative phase, and the climate in Patagonia dramatically changed again. The proxy climate records from the pollen assemblages and mineral compositions indicate that northern Patagonia became wetter (Lamy et al., 1999; Jara and Moreno, 2014; Moreno et al., 2018;

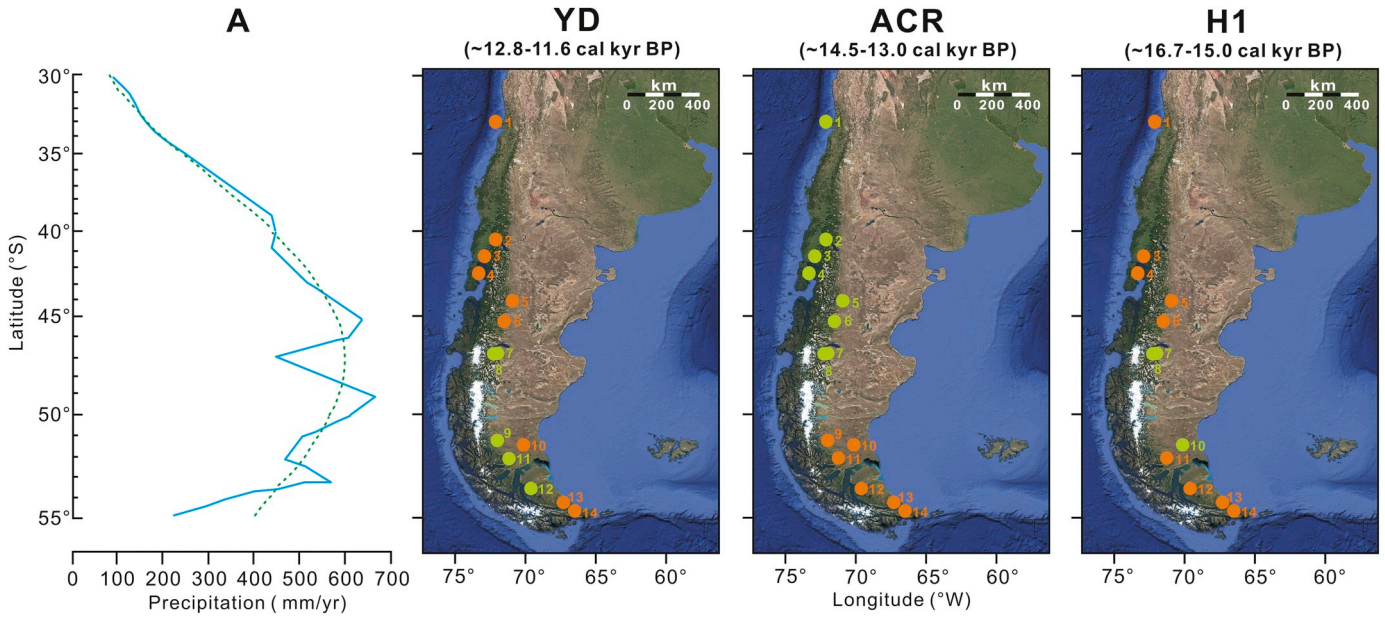

Fig. 4. The regional distribution patterns of the dry and wet climate in the southern South America during the last glacial–interglacial transition. Panel H1–The dry and wet distribution pattern during the Heinrich event 1 (H1). Panel ACR–The dry and wet distribution pattern during the Antarctic Cold Reversal (ACR). Panel YD–The dry and wet distribution pattern during the Younger Dryas (YD). Panel A–The latitudinal distribution of modern annual rainfall in Western Chile, in which a dashed line is the normal best fit to the annual rainfall amounts (modified from Quade and Kaplan, 2017). Green dot represents a wetter climate. Red dot represents a drier climate. The relevant data on the research sites 1–14, including the position coordinates, proxy climate indicators, dating, climate condition, and the author and the source of the original literature, are listed in Table 1. Site 1–Geob 3302–1 core (Lamy et al., 1999). Site 2–Lago Pichilafquén (Jara and Moreno, 2014). Site 3–Lago Pichilaguna (Moreno et al., 2018). Site 4–Lago Lepué (Pesce and Moreno, 2014). Site 5–Lago Los Niños (Iglesias et al., 2016). Site 6–Mallín Pollux (Markgraf et al., 2007). Site 7–Lago Augusta (Villa-Martínez et al., 2012). Site 8–Lago Edita (Henríquez et al., 2017). Site 9–Pantano Dumestre (Moreno et al., 2012). Site 10–Laguna Potrok Aike (Wille et al., 2007). Site 11–Rio Rubens (Markgraf and Uber, 2010). Site 12–Punta Yartou core (Mansilla et al., 2016). Site 13–La Correntina mire (Musotto et al., 2017). Site 14–Harberton (Markgraf and Uber, 2010). Sites 2 and 9 are not shown in panel H1, because the original records in Jara and Moreno, 2014 and Moreno et al., 2012 did not provide the climate data during the H1 event. (For interpretation of the references to colour in this figure legend, the reader is referred to the web version of this article.)

Pesce and Moreno, 2014; Iglesias et al., 2016; Markgraf et al., 2007; Villa-Martínez et al., 2012; Henríquez et al., 2017) (Sites 1–8 in Fig. 4) while South Patagonia became drier (Moreno et al., 2012; Wille et al., 2007; Markgraf and Uber, 2010; Mansilla et al., 2016; Musotto et al., 2017) (Sites 9–14 in Fig. 4) during the period of the ACR event or the time interval roughly equivalent to the ACR event (panel ACR in Fig. 4). We interpret this regional differentiation in climate as a consequence of the equatorward shift of the SWW. The boundary between the dry and the humid areas may be located at approximately 47°S. During this period, the northern edge of the SWW may have expanded to approximately 33°S, which is more north than the corresponding location in the late LGM, while the southern margin of the SWW may be located at approximately 47°S. The northern region of Patagonia influenced by the SWW is wider, covering approximately 14 degrees of latitude. The mean latitudinal position of the core of the SWW may have been located at approximately 40°S, which obviously deviated northward from the core position of the modern SWW (panels ACR and A in Fig. 4), leading to drier conditions in southern Patagonia.

Accompanied by another large amount of meltwater discharge into the North Atlantic Ocean, the YD cooling event occurred in the NH (Broecker, 1994; Alley et al., 1999). The panel YD in Fig. 4 shows that during the YD or the time interval roughly equivalent to the YD event, northern Patagonia (Lamy et al., 1999; Jara and Moreno, 2014; Moreno et al., 2018; Pesce and Moreno, 2014; Iglesias et al., 2016; Markgraf et al., 2007) (Sites 1–6 in Fig. 4) and the southernmost part of Patagonia (Musotto et al., 2017; Markgraf and Uber, 2010) (Sites 13,14 in Fig. 4) became drier again, and the region of south central Patagonia (Villa-Martínez et al., 2012; Henríquez et al., 2017; Moreno et al., 2012; Markgraf and Uber, 2010; Mansilla et al., 2016) (Sites 7–9,11,12 in Fig. 4) between approximately 47° and 54°S became wetter in general, although there are exceptions in individual areas (Wille et al., 2007) (Site 10 in Fig. 4). The regional distribution pattern of climate may again reflect the southward shift of the SWW, which is similar to phenomenon that occurred in the H1 event, but its southern border in the YD period was closer to the Antarctic continent than during the periods of the modern and H1 events.

Although the abovementioned regional changes in the dry and wet conditions are usually interpreted as the result of the north–south migration of the mean latitudinal position of the SWW, we have further observed new important phenomena. As shown in panels H1, ACR, and YD in Fig. 4, during the last glacial-interglacial transition, the mountainous regions of the Andes at approximately 47°S (represented by Sites 7 and 8 Fig. 4) have been wetter at all times (Villa-Martínez et al., 2012; Henríquez et al., 2017), showing the stable region in the shifting SWW that is consistent with the core position of the modern westerly wind. In response to the positive TCBH, the SWW extends poleward from the 47°S region, with a relatively smaller amplitude. However, in response to the negative TCBH, the SWW expands equatorward from the 47°S region and has a larger amplitude. Therefore, the position change of the SWW seems to behave as a swing process in the direction and amplitude with an axis of approximately 47°S (Fig. 5D). This mode of change is different from the north–south migration of the whole SWW, which deserves further comparative study.

3.3. *Concurrent changes of the ISM and the SWW and their feedback to the TCBH*

Fig. 5 shows, for the first time, responses of the ISM and the SWW to the TCBH and the concurrent changes of the ISM and the SWW during the last glacial–interglacial transition. When the meltwater flood events occurred in the high northern latitudes during the time intervals from approximately 16,700 to 15,000 cal kyr BP (i.e., the H1 event) and from

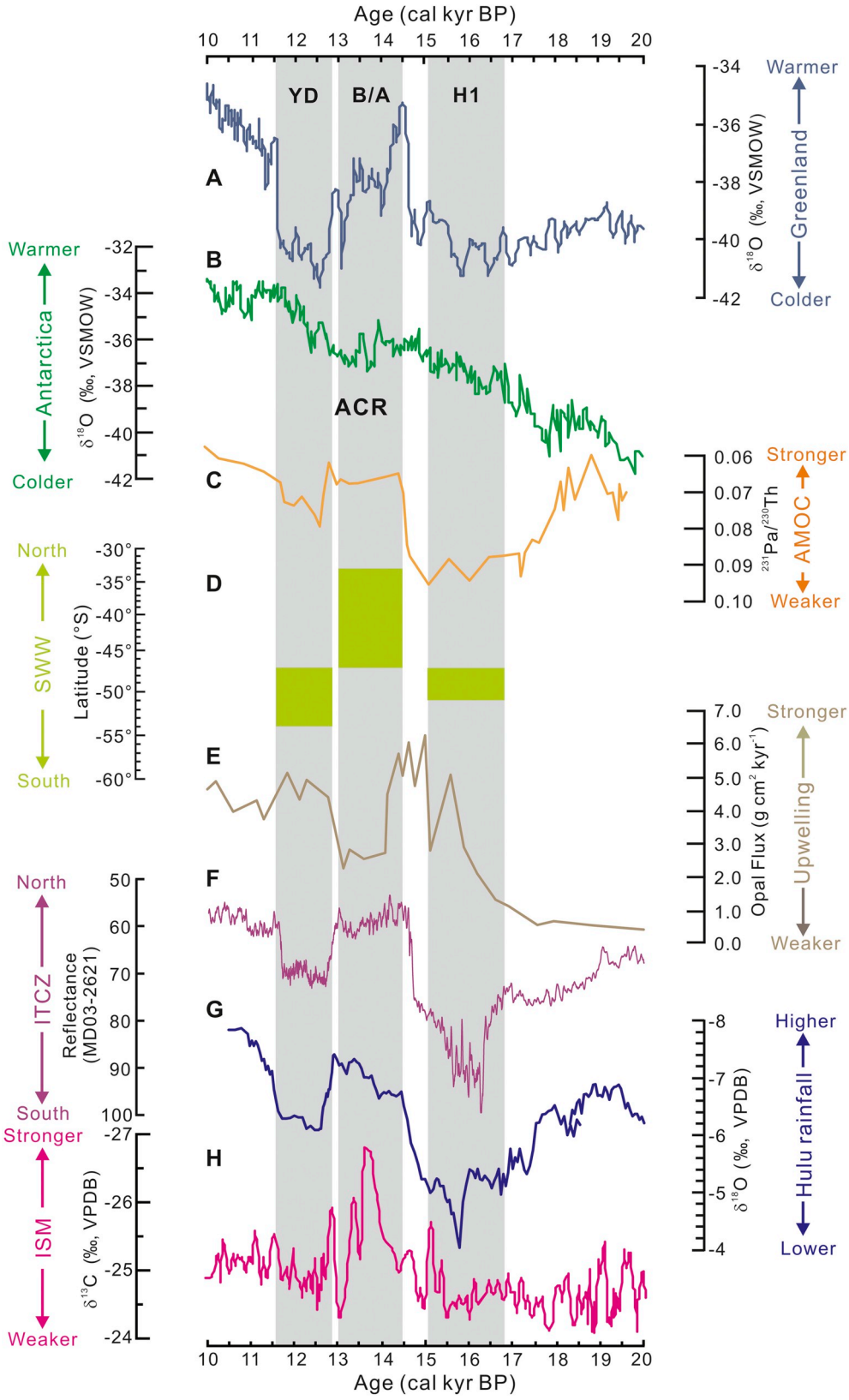

Fig. 5. Responses of the Indian summer monsoon (ISM), the Southern Westerly Winds (SWW), and the Intertropical Convergence Zone (ITCZ) to a temperature contrast between the hemispheres (TCBH) during the last deglaciation. A–Temperature record reconstructed from the $\delta^{18}O$ of the GISP2 ice core in Greenland (Stuiver and Grootes, 2000). B–Temperature record reconstructed from the $\delta^{18}O$ of the Byrd ice core in Antarctica (Blunier and Brook, 2001). The comparison of temperature records A and B reflects the condition of TCBH. C–The $^{231}Pa/^{230}Th$ record in sediment from Bermuda rise in the subtropical North Atlantic Ocean (McManus et al., 2004). D–The core positions of the SWW inferred from the panels H1, ACR, and YD in Fig. 4, respectively (this study). E–Biogenic opal flux record from TN057–13-4PC core in the Southern Indian Ocean (Anderson et al., 2009) (Site 5 in Fig. 1). F–The position of the ITCZ over the Cariaco Basin (Deplazes et al., 2013). G–The $\delta^{18}O$ record from stalagmites in Hulu Cave (Wang et al., 2001). H–The $\delta^{13}C$ record from cellulose of Yuexi peat (Hong et al., 2018). The climatic intervals are abbreviated as follows: YD–Younger Dryas; B/A–Bølling/Allerød; ACR–Antarctic Cold Reversal; AMOC–the Atlantic meridional overturning circulation. The grey bars indicate the H1, the ACR/the B/A, and the YD events.

12,800 to 11,600 cal kyr BP (i.e., the YD event), respectively, the AMOC inferred from the $^{231}Pa/^{230}Th$ in sediment measured from Bermuda was nearly or completely eliminated (McManus et al., 2004) (Fig. 5C). Moreover, the positive TCBH was established (Figs. 5A and B), which may further lead to the southward or poleward shifts of the ITCZ over the South American and Asian continents (Fig. 5F). The SWW swung poleward from the 47°S region (Fig. 5D); and the ISM intensity weakened (Figs. 5G and H). The above results provide clear and coherent evidence for the simultaneous occurrence of these physical processes, supporting the hypothesis that the positive TCBH drives global climate

changes such as the NH forcing of the SH climate (Anderson et al., 2009; Denton et al., 2010; Broecker, 1994; Chiang and Friedman, 2012; He et al., 2013).

In this process, however, whether the SH also affects the NH is still open for discussion. Based on the satellite data of the SST in global night-time, Sirocko (2003) discussed the potentially important role of climate processes in the SH, especially the SWW, for the global climate changes. Denton et al. (2010) suggested that the southward shift of the SWW was one of the essential elements causing the sudden warming of a long-time cooling climate during the deglaciation (Fig. 3 in Denton et al., 2010), although there were no data for the SWW shift in Fig. 4 of Danton et al. at the time. In addition, the SWW-driven upwelling brings Circumpolar Deep Water to the surface, leading not only to the influence of deep-water circulation in the Southern Ocean, but also to the release of CO_2 from the deep sea into the atmosphere (Anderson et al., 2009). Previous studies have also suggested that the upwelling in the Southern Ocean is the upwelling branch of the AMOC (Marshall and Speer, 2012). The combined action of the Southern Ocean upwelling and the North Atlantic downwelling completes the closure of the AMOC (Marshall and Speer, 2012). Therefore, we consider that the enhanced upwelling caused by the SWW swing southward (Toggweiler et al., 2006) should also reflect the enhanced pulling effect of the SWW on the AMOC. In the case of the H1 event, under the combined action of the pulling force of the SWW, which lasted for approximately 1700 years (i.e., from approximately 16,700 to 15,000 cal kyr BP), and the increase in the accompanying atmospheric CO_2 concentration, the global climate system would eventually cross a certain threshold state and start to restore the active operation of the AMOC. As shown in Fig. 5, for approximately 600 years, i.e., from 15,100 to 14,500 cal kyr BP after the completion of the H1 event, accompanied by a rapid increase and a maximum value of the southern upwelling (Fig. 5E), the gradual strengthening of the AMOC (as indicated by the $^{231}Pa/^{230}Th$ ratio (McManus et al., 2004) (Fig. 5C)), the gradual increase of CO_2 concentration in the atmosphere (Monnin et al., 2001), and the gradual strengthening of the ISM leading to transport of more heat to the NH (Fig. 5H), the TCBH was converted from the positive phase to the negative phase (Figs. 5A and B). Finally, the Earth's climate entered the NH -wide warming and the SH-wide cooling period that is the period of the B/A or the ACR. During that period, the ITCZ over the South American and Asian continents shifted northward or equatorward (Fig. 5F), the SWW swung equatorward from the 47°S region (Fig. 5D), and the ISM strengthened (Figs. 5G and H). This climate pattern was obviously different from the climate pattern during the H1 event until the next large meltwater outburst occurred; this next event was the YD event. We consider that the phase changes of the TCBH and the subsequent responses of the ISM and the SWW may reflect the stress-related changes and the self-repair processes of the Earth's climate system to the catastrophic impact of meltwater floods, which suggests that there is a process of interaction between the NH and SH. In addition to the NH driving the SH, the SH could also drive the NH, which constitutes the two aspects of the response process of the climate system to the catastrophic impact of meltwater. Our results mentioned above highlight the importance of the SWW in the climate teleconnection between the NH and SH. The concurrent changes of the ISM and the SWW on the millennium timescales may make it possible to assess the variation trends of the SWW and its associated climatic processes based on the ISM information.

4. Conclusions

The responses of the ITCZ position shift to the TCBH phase changes during the last deglaciation are further discussed in this paper. We suggest that the zonal-mean position shifts of the ITCZ over the Asian and the northern South American continents on the two sides of the Pacific Ocean are synchronous. Furthermore, the directions of their shifts are the same. In response to the positive (negative) TCBH, southward (northward) shifts of the ITCZ over these continents occur, while the intensity of the ISM decreases (increases). However, little is been known about the magnitude and direction of the ITCZ shift over the vast Pacific Ocean during the last deglaciation. The change in the intensity of the East Asian summer monsoon related to water vapour from the Pacific Ocean has been reported to be contrary to the change in the intensity of the ISM. Whether this inverse phase correlation between the two monsoons implies the opposite shift of the ITCZ over the Pacific and Indian Oceans deserves further confirmation because this opposite change may affect the assessment of the magnitude and direction of global mean displacement of the ITCZ. In addition, considering that this inverse correlation may be related to the El Niño-like activities in the tropical Pacific, it is necessary to clarify the relationship between the ENSO-like phenomenon and TCBH.

This study shows that in the process of the SWW shift during the last glacial–interglacial transition, there may be a relatively stable core region of the SWW. This core region is located in Central Patagonia at approximately 47°S, where the local climate is wetter during the all transition period, which shows the continuous influence of the SWW on this region. In particular, this core region of the SWW during the last glacial–interglacial transition is almost consistent with the core position of the modern SWW. In response to the positive TCBH (or in the H1 event), the SWW extends poleward from the 47°S region, with a relatively smaller amplitude. However, in response to the negative TCBH (or in the ACR event), the SWW expands equatorward from the 47°S region and has a larger amplitude. When the positive TCBH (or in the YD event) appears again, the SWW extends poleward from the 47°S region again. Therefore, the position shift of the SWW in response to the TCBH changes seems to behave as a swing in the direction and amplitude with an axis of approximately 47°S. This mode of shift differs from the north–south displacement of the whole SWW.

In response to the impacts of the catastrophic meltwater discharge, or to the positive TCBH, the southward shifts of both the ITCZ and the SWW occurred. It is likely that the poleward expansion of the SWW may trigger the self-repairing process of the climate system on the catastrophic impacts of the meltwater because the SWW near the Antarctic continent will enhance the upwelling in the Southern Ocean, which will not only help to release more CO_2 in the deep sea of the Southern Ocean into the atmosphere but also enhance the pulling effect on the AMOC, eventually leading to the transformation of the TCBH from the positive phase to the negative phase and the northward shifts of the ITCZ and the SWW. This scenario highlights that the SWW may play an important role in global climate change, especially in the impact of the SH on the NH. The Earth's climate system shows the ability to self-repair the impacts of some catastrophic events in the history of geology. However, whether the climate system can cope with the impacts of modern human activities remains a challenging research topic.

Competing financial interests

The authors declare no conflict of interest.

Acknowledgements

This work was supported by the National Natural Science Foundation of China (Grant No. 41673119, 41773140, 41373134).

References

Alley, R., Clark, P.U., Keigwin, L.D., Webb, R.S., 1999. Making sense of millennial-scaleclimatechange. In: Clark, P.U., Webb, R.S., Keigwin, L.D. (Eds.), Mechanisms of Global Climate Change at Millennial Time Scalesn. Geophys. Monogr. Ser, vol. 112. AGU, Washington, D. C, pp. 385–394.

Amesbury, M.J., Charman, D.J., Newnham, R.M., Loader, N.J., Goodrich, J.P., Royles, J., Campbell, D.I., Roland, T.P., Gallego-Sala, A., 2015. Carbon stable isotopes as a palaeoclimate proxy in vascular plant dominated peatlands. Geochim. Cosmochim. Acta 164, 161–174.

Anderson, R.F., Ali, S., Bradtmiller, L.I., Nielsen, S.H.H., Fleisher, M.Q., Anderson, B.E., Burckle1, L.H., 2009. Wind-driven upwelling in the Southern Ocean and the deglacial rise in atmospheric CO_2. Science 323, 1443–1448.

Ayliffe, L.K., Gagan, M.K., Zhao, J.-x., Drysdale, R.N., Hellstrom, J.C., Hantoro, W.S., Griffiths, M.L., Scott-Gagan, H., Pierre, E.S., Cowley, J.A., Suwargadi, B.W., 2013. Rapid interhemispheric climate links via the Australasian monsoon during the last deglaciation. Nat. Commun. 4, 2908. https://doi.org/10.1038/ncomms3908.

Barker, S., Diz, P., Vautravers, M.J., Pike, J., Knorr, G., Hall, I.R., Broecker, W.S., 2009. Interhemispheric Atlantic seesaw response during the last deglaciation. Nature 457, 1097–1102.

Blunier, T., Brook, E.J., 2001. Timing of millennial-scale climate change in Antarctica and Greenland during the last glacial period. Science 291, 109–112.

Broecker, W.S., 1994. Massive iceberg discharges as triggers for global climate change. Nature 372, 421–424.

Broecker, W.S., Peteet, D.M., Rind, D., 1985. Does the ocean-atmosphere system have more than one stable mode of operation? Nature 315, 21–26.

Buckley, B.M., Anchukaitis, K.J., Penny, D., Fletcher, R., Cook, E.R., Sano, M., Nam, L.C., Wichienkeeo, A., Minh, T.T., Hong, T.M., 2010. Climate as a contributing factor in the demise of Angkor, Cambodia. P. Natl. Acad. Sci. USA 107, 6748–6752.

Byrne, M.P., Pendergrass, A.G., Rapp, A.D., Wodzicki, K.R., 2018. Response of the intertropical convergence zone to climate change: location, width, and strength. Curr. Clim. Chang. Rep. 4, 355–370. https://doi.org/10.1007/s40641-018-0110-5.

Carolin, S.A., Cobb, K.M., Adkins, J.F., Clark, B., Conroy, J.L., Lejau, S., Malang, J., Tuen, A.A., 2013. Varied response of western Pacific hydrology to climate forcings over the last glacial period. Science 340, 1564–1566.

Cheng, H., Sinha, A., Wang, X.F., Cruz, F.W., Edwards, R.L., 2012. The Global Paleomonsoon as seen through speleothem records from Asia and the Americas. Clim. Dyn. 39, 1045–1062.

Chiang, J.C.H., Friedman, A.R., 2012. Extratropical cooling, interhemispheric thermal gradients, and tropical climate change. Annu. Rev. Earth Planet. Sci. 40, 383–412.

Denniston, R.F., Wyrwoll, K.-H., Asmerom, Y., Polyak, V.J., Humphreys, W.F., Cugley, J., Woods, D., LaPointe, Z., Peota, J., Greaves, E., 2013. North Atlantic forcing of millennial-scale Indo-Australian monsoon dynamics during the Last Glacial period. Quat. Sci. Rev. 72, 159e168.

Denton, G.H., Anderson, R.F., Toggweiler, J.R., Edwards, R.L., Schaefer, J.M., Putnam, A.E., 2010. The last glacial termination. Science 328, 1652–1656.

Deplazes, G., Lückge, A., Peterson, L.C., Timmermann, A., Hamann, Y., Hughen, K.A., Röhl, U., Laj, C., Cane, M.A., Sigman, D.M., Haug, G.H., 2013. Links between tropical rainfall and North Atlantic climate during the last glacial period. Nat. Geosci. 6, 213–217.

Dykoski, C.A., Edwards, R.L., Cheng, H., Yuan, D.X., Cai, Y.J., Zhang, M.L., Lin, Y.S., Qing, J.M., An, Z.S., Revenaugh, J., 2005. A high-resolution absolute-dated Holocene and deglacial Asian monsoon record from Dongge Cave, China. Earth Planet. Sci. Lett. 233, 71–86.

Fleitmann, D., Burns, S.J., Mudelsee, M., Neff, U., Kramers, J., Mangini, A., Matter, A., 2003. Holocene forcing of the Indian monsoon recorded in a stalagmite from Southern Oman. Science 300, 1737–1739.

Fleitmann, D., Burnsb, S.J., Manginic, A., Mudelseed, M., Kramersa, J., Villaa, I., Neffc, U., Al-Subbarye, A.A., Buettnera, A., Hipplera, D., Mattera, A., 2007. Holocene ITCZ and Indian monsoon dynamics recorded in stalagmites from Oman and Yemen (Socotra). Quat. Sci. Rev. 26, 170–188.

Fletcher, M.-S., Moreno, P.I., 2011. Zonally symmetric changes in the strength and position of the Southern Westerlies drove atmospheric CO_2 variations over the past 14 k.y. Geology 39, 419–422.

Fraser, N., Kuhnt, W., Holbourn, A., Bolliet, T., Andersen, N., Blanz, T., Beaufort, L., 2014. Precipitation variability within the West Pacific warm pool over the past 120 ka: evidence from the Davao Gulf, southern Philippines. Paleoceanography 29, 1094e1110.

Gao, Y.X., Xu, S.Y., Guo, Q.Y., 1962. Monsoon region and regional climate in China. In: Gao, Y.X., Xu, S.Y. (Eds.), Some Problems of East Asian Monsoon. Science Press, Beijing, pp. 49–63.

Garreaud, R.D., 2007. Precipitation and circulation covariability in the extratropics. J. Clim. 20, 4789–4797.

Griffiths, M.L., Drysdale, R.N., Gagan, M.K., Zhao, J.X., Ayliffe, L.K., Hellstrom, J.C., Hantoro, W.S., Frisia, S., Feng, Y.X., Cartwright, I., Pierre, E.S., Fischer, M.J., Suwargadi, B.W., 2009. Increasing Australian-Indonesian monsoon rainfall linked to early Holocene sea-level rise. Nat. Geosci. 2, 636–639.

Gupta, A.K., Anderson, D.M., Overpeck, J.T., 2003. Abrupt changes in the Asian southwest monsoon during the Holocene and their links to the North Atlantic Ocean. Nature 421, 354–357.

He, F., Shakun, J.D., Clark, P.U., Carlson, A.E., Liu, Z., Otto-Bliesner, B.L., Kutzbach, J.E., 2013. Northern Hemisphere forcing of Southern Hemisphere climate during the last deglaciation. Nature 494, 81–85.

Henríquez, W.I., Villa-Martínez, R., Vilanova, I., De Pol-Holz, R., Moreno, P.I., 2017. The last glacial termination on the eastern flank of the central Patagonian Andes (47° S). Clim. Past 13, 879–895.

Hong, Y.T., Wang, Z.G., Jiang, H.B., Lin, Q.H., Hong, B., Zhu, Y.X., Wang, Y., Xu, L.S., Leng, X.T., Li, H.D., 2001. A 6000-year record of changes in drought and precipitation in northeastern China based on a $\delta^{13}C$ time series from peat cellulose. Earth Planet. Sci. Lett. 185, 111–119.

Hong, Y.T., Hong, B., Lin, Q.H., Zhu, Y.X., Shibata, Y., Hirota, M., Uchida, M., Leng, X.T., Jiang, H.B., Xu, H., Wang, H., Yi, L., 2003. Correlation between Indian Ocean summer monsoon and North Atlantic climate during the Holocene. Earth Planet. Sci. Lett. 211, 371–380.

Hong, Y.T., Hong, B., Lin, Q.H., Shibata, Y., Hirota, M., Zhu, Y.X., Leng, X.T., Wang, Y., Wang, H., Yi, L., 2005. Inverse phase oscillations between the East Asian and Indian Ocean summer monsoons during the last 12000 years and paleo-El Niño. Earth Planet. Sci. Lett. 231, 337–346.

Hong, Y.T., Hong, B., Lin, Q.H., Shibata, Y., Zhu, Y.X., Leng, X.T., Wang, Y., 2009. Synchronous climate anomalies in the western North Pacific and North Atlantic regions during the last 14,000 years. Quat. Sci. Rev. 28, 840–849.

Hong, B., Hong, Y.T., Lin, Q.H., Shibata, Y., Uchida, M., Zhu, Y.X., Leng, X.T., Wang, Y., Cai, C.C., 2010. Anti-phase oscillation of Asian monsoons during the Younger Dryas period: evidence from peat cellulose $\delta^{13}C$ of Hani, Northeast China. Paleogeogr. Paleoclimatol. Paleoecol. 297, 214–222.

Hong, B., Hong, Y.T., Uchida, M., Leng, X.T., Shibata, Y., Cai, C., Peng, H.J., Zhu, Y.X., Wang, Y., Yuan, L.G., 2014. Abrupt variations of Indian and East Asian summer monsoons during the last deglacial stadial and interstadial. Quat. Sci. Rev. 97, 58–70.

Hong, B., Uchida, M., Hong, Y.T., Peng, H.J., Kondo, M., Guo, Q., Ding, W.H., Yao, H., Xu, C., 2018. The respective characteristics of millennial-scale changes of the India summer monsoon in the Holocene and the Last Glacial. Palaeogeogr. Palaeoclimatol. Palaeoecol. 496, 155–165.

Iglesias, V., Markgraf, V., Whitlock, C., 2016. 17,000 years of vegetation, fire and climate change in the eastern foothills of the Andes (lat. 44°S). Palaeogeogr. Palaeoclimatol. Palaeoecol. 457, 195–208.

Jara, I.A., Moreno, P.I., 2014. Climatic and disturbance influences on the temperate rainforests of northwestern Patagonia (40°S) since ~14,500 cal yr BP. Quat. Sci. Rev. 90, 217–228.

Knutti, R., Fluckiger, J., Stocker, T.F., Timmermann, A., 2004. Strong hemispheric coupling of glacial climate through freshwater discharge and ocean circulation. Nature 430, 851–856.

Kohfeld, K.E., Graham, R.M., de Boer, A.M., Sime, L.C., Wolff, E.W., Quéré, C. Le, Bopp, L., 2013. Southern Hemisphere westerly wind changes during the Last Glacial Maximum: paleo-data synthesis. Quat. Sci. Rev. 68, 76–95.

Koutavas, A., Lynch-Stieglitz, J., Marchitto, T.M., Sachs, J.P., 2002. El Niño-like pattern in Ice Age tropical Pacific sea surface temperature. Science 297, 226–230.

Kumar, K.K., Rajagopalan, B., Hoerling, M., Bates, G., Cane, M., 2006. Unraveling the mystery of Indian monsoon failure during El Niño. Science 314, 115–119.

Lamy, F., Hebbeln, D., Wefer, G., 1999. High-resolution marine record of climatic change in mid-latitude Chile during the last 28,000 years based on terrigenous sediment parameters. Quat. Res. 51, 83–93.

Landais, A., Masson-Delmotte, V., Stenni, B., Selmo, E., Roche, D.M., Jouzel, J., Lambert, F., Guillevic, M., Bazin, L., Arzel, O., Vinther, B., Gkinis, V., Popp, T., 2015. A review of the bipolar seeesaw from synchronized and high resolution ice core water stable isotope records from Greenland and East Antarctica. Quat. Sci. Rev. 114, 18–32.

Lawford, R.G., Lawford, R.G., et al., 1996. North-South variations in west coast hydrometeorological parameters and their significance for Earth systems. In: Highelatitude Rainforests and Associated Ecosystems of the West Coast of America. Springer -Verlag, New York, pp. 3–26.

Maher, B.A., Hu, M.Y., 2006. A high-resolution record of Holocene rainfall variations from the western Chinese Loess Plateau: antiphase behaviour of the African/Indian and East Asian summer monsoons. The Holocene 16 (3), 309–/319.

Mansilla, C.A., McCulloch, R.D., Morello, F., 2016. Palaeoenvironmental change in Southern Patagonia during the Lateglacial and Holocene: implications for forest refugia and climate reconstructions. Palaeogeogr. Palaeoclimatol. Palaeoecol. 447, 1–11.

Markgraf, V., Uber, U.M., 2010. Late and postglacial vegetation and fire history in southern Patagonia and Tierra del Fuego. Palaeogeogr. Palaeoclimatol. Palaeoecol. 297, 351–366.

Markgraf, V., Whitlock, C., Haberle, S., 2007. Vegetation and fire history during the last 18,000 cal yr B.P. in Southern Patagonia: Mallín Pollux, Coyhaique, Province Aisén (45°41′30″ S, 71°50′30″ W, 640m elevation). Palaeogeogr. Palaeoclimatol. Palaeoecol. 254, 492–507.

Marshall, J., Speer, K., 2012. Closure of the meridional overturning circulation through Southern Ocean upwelling. Nat. Geosci. 5, 171–180.

McGee, D., Donohoe, A., Marshall, J., Ferreira, D., 2014. Changes in ITCZ location and cross-equatorial heat transport at the Last Glacial Maximum, Heinrich stadial 1, and the mid-Holocene. Earth Planet. Sci. Lett. 390, 69–79.

McManus, J.F., Francoi,s, R., Gherardi, J.-M., Keigwin, L.D., Brown-Leger, S., 2004. Collapse and rapid resumption of Atlantic meridional circulation linked to deglacial climate changes. Nature 428, 834–837.

Meehl, G.A., Hu, A., 2006. Megadroughts in the Indian monsoon region and southwest North America and a mechanism for associated multidecadal pacific sea temperature anomalies. J. Clim. 19, 1605–1623.

Mohtadi, M., Prange1, M., Steinke1, S., 2016. Palaeoclimatic insights into forcing and response of monsoon rainfall. Nature 533, 191–199.

Monnin, E., Indermühle, A., Dallenbach, A., Flückiger, J., Stauffer, B., Stocker, T.F., Raynaud, D., Jean-Marc Barnola, J.-M., 2001. Atmospheric CO_2 concentrations over the Last Glacial termination. Science 291, 112–114.

Moreno, P.I., Lowell, T.V., Jacobson, G.L., Denton, G.H., 1999. Abrupt vegetation and climate changes during the last glacial maximum and last termination in the Chilean lake district: a case study from Canal de Puntilla (41°S). Geogr. Ann. 81A, 285–311.

Moreno, P.I., Villa-Martínez, R., Cárdenas, M.L., Sagredo, E.A., 2012. Deglacial changes of the southern margin of the southern westerly winds revealed by terrestrial records from SW Patagonia (52°S). Quat. Sci. Rev. 41, 1–21.

Moreno, P.I., Videla, J., Valero-Garcés, B., Alloway, B.V., Heusser, L.E., 2018. A continuous record of vegetation, fire-regime and climatic changes in northwestern Patagonia spanning the last 25,000 years. Quat. Sci. Rev. 198, 15–36.

Muller, J., Kylander, M., Wüst, R.A.J., Weiss, D., Martinez-Cortizas, A., LeGrande, A.N., Jennerjahn, T., Behling, H., Anderson, W.T., Jacobson, G., 2008. Possible evidence for wet Heinrich phases in tropical NE Australia: the Lynch's Crater deposit. Quat. Sci. Rev. 27, 468–475.

Musotto, L.L., Borromei, A.M., Bianchinotti, M.V., Coronato, A., 2017. Late Quaternary palaeoenvironmental reconstruction of central Tierra del Fuego (Argentina) based on pollen and fungi. Quat. Int. 442 A 23, 13–25.
Pausata, F.S.R., Battisti, D.S., Nisancioglu, K.H., Bitz, C.M., 2011. Chinese stalagmite $\delta^{18}O$ controlled by changes in the Indian monsoon during a simulated Heinrich event. Nat. Geosci. 4, 474–480 (2011).
Pesce, O.H., Moreno, P.I., 2014. Vegetation, fire and climate change in central-east Isla Grande de Chiloé (43°S) since the Last Glacial Maximum, northwestern Patagonia. Quat. Sci. Rev. 90, 143–157.
Quade, J., Kaplan, M.R., 2017. Lake-level stratigraphy and geochronology revisited at Lago (Lake) Cardiel, Argentina, and changes in the Southern Hemispheric Westerlies over the last 25 ka. Quat. Sci. Rev. 177, 173–188.
Schneider, T., Bischoff, T., Haug, G.H., 2014. Migrations and dynamics of the intertropical convergence zone. Nature 513, 45–53.
Schulz, H., Von Rad, U., Erlenkeuser, H., 1998. Correlation between arabian sea and Greenland climate oscillations of the past 110,000 years. Nature 393, 54–57.
Shiau, L.J., Chen, M.T., Clemens, S.C., Huh, C.A., Yamamoto, M., Yokoyama, Y., 2011. Warm pool hydrological and terrestrial variability near southern Papua New Guinea over the past 50k. Geophys. Res. Lett. 38, L00F01. https://doi.org/10.1029/2010GL045309.
Shukla, J., Paolina, D., 1983. The Southern Oscillation and long range forecasting of the summer monsoon rainfall over India. Mon. Weather Rev. 111, 1830–1837.
Sirocko, F., 2003. What drove past teleconnections? Science 301, 1336–1337.
Stager, J.C., Ryves, D.B., Chase, B.M., Pausata, F.S.R., 2011. Catastrophic drought in the Afro-Asian monsoon region during Heinrich event 1. Science 331, 1299–1302.
Stott, L., Poulsen, C., Lund, S., Thunell, R., 2002. Supper ENSO and global climate oscillations at millennial time scales. Science 297, 222–226.
Stuiver, M., Grootes, P.M., 2000. GISP2 oxygen isotope rations. Quat. Res. 53, 277–283.
Timmermann, A., Okumura, Y., An, S.I., Clement, A., Dong, B., Guilyardi, E., Hu, A., Jungclaus, J.H., Renold, M., Stocker, T.F., Stouffer, R.J., Sutton, R., Xie, S.-P., Yin, J., 2007. The influence of a weakening of the Atlantic meridional overturning circulation on ENSO. J. Clim. 20, 4899–4919.
Toggweiler, J.R., 2009. Shifting westerlies. Science 323, 1434–1435.
Toggweiler, J.R., Russell, J.L., Carson, S.R., 2006. Midlatitude westerlies, atmospheric CO_2, and climate change during the ice ages. Paleoceanography 21https://doi.org/10.1029/2005PA001154. PA2005.
Villa-Martínez, R., Moreno, P.I., Valenzuela, M.A., 2012. Deglacial and postglacial vegetation changes on the eastern slopes of the central Patagonian Andes (47°S). Quat. Sci. Rev. 32, 86–99.
Wang, H.J., Chen, H.P., 2012. Climate control for southeastern China moisture and precipitation: Indian or East Asian monsoon? J. Geophys. Res. 117, D12109. https://doi.org/10.1029/2012JD017734.
Wang, Y.J., Cheng, H., Edwards, R.L., An, Z.S., Wu, J.Y., Shen, C.-C., Dorale, J.A., 2001. A high-resolute absolute-dated Late Pleistocene monsoon record from Hulu Cave, China. Science 294, 2345–2348.
Wang, Y., Cheng, H., Edwards, R.L., He, Y., Kong, X., Zhisheng, A., Wu, J., Kelly, M.J., Dykoski, C.A., Li, X., 2005. The Holocene Asian monsoon: links to solar changes and North Atlantic climate. Science 308, 854–857.
Webster, P.J., Magana, V.O., Palmer, T.N., Shukla, J., Tomas, R.A., Yanai, M., Yasunari, T., 1998. Monsoons: processes, predictability, and the prospects for prediction. J. Geophys. Res. 103, 14451–14510.
Wille, M., Maidana, N.I., Schäbitz, F., Fey, M., Haberzettl, T., Janssen, S., Lücke, A., Mayr, C., Ohlendorf, C., Schleser, G.H., Zolitschka, B., 2007. Vegetation and climate dynamics in southern South America: the microfossil record of Laguna Potrok Aike, Santa Cruz, Argentina. Rev. Palaeobot. Palynol. 146, 234–246.
Xiong, Z.F., Li, T.G., Chang, F.M., Algeo, T.J., Clift, P.D., Bretschneider, L., Lu, Z.Y., Zhu, X., Frank, M., Sauer, P.E., Jiang, F.Q., Wan, S.M., Zhang, X., Chen, S.X., Jie Huang, J., 2018. Rapid precipitation changes in the tropical West Pacific linked to North Atlantic climate forcing during the last deglaciation. Quat. Sci. Rev. 197, 288–306.
Yuan, D.X., Cheng, H., Edwards, R.L., Dykoski, C.A., Kelly, M.J., Zhang, M.L., Qing, J.M., Lin, Y.S., Wang, Y.J., Wu, J.Y., Dorale, J.A., An, Z.S., Cai, Y.J., 2004. Timing, duration, and transitions of the last interglacial Asian monsoon. Science 304, 575–578.